Design and analysis of superlens based on complex two-dimensional square lattice photonic crystal

Somayeh Rafiee Dastjerdi[1], Majid Ghanaatshoar[1*], and Toshiaki Hattori[2]

[1]*Laser and Plasma Research Institute, Shahid Beheshti University, G.C., Evin 1983963113, Tehran, Iran*

[2]*Institute of Applied Physics, University of Tsukuba, Tsukuba 305-8573, Japan*

[*]*Corresponding author: m-ghanaat@sbu.ac.ir*

Received June 6, 2013; accepted August 14, 2013; posted online September 30, 2013

We theoretically demonstrate the imaging properties of a complex two-dimensional (2D) face-centered square lattice photonic crystal (PC) made from germanium cylinders in air background. The finite-difference time-domain (FDTD) method is employed to calculate the band structure and simulate image construction. The band diagram of the complex structure is significantly compressed. Negative refraction occurs in the second energy band with negative phase velocity at a frequency of 0.228 ($2\pi c/a$), which is lower than results from previous studies. Lower negative refraction frequency leads to higher image resolution. Numerical results show that the spatial resolution of the system reaches 0.7296λ, which is lower than the incident wavelength.

OCIS codes: 230.5298, 100.6640, 130.3120, 060.4510.

doi: 10.3788/COL201311.102303.

Negative refractive index materials (NIMs) or left-handed materials (LHMs) have received considerable attention because of their interesting properties such as negative refraction and subwavelength imaging. Typical NIMs have simultaneous negative permeability and permittivity, which are initially suggested by Veselago in 1968[1]. Given that NIMs were not readily available in nature, these materials were not paid much attention until Pendry presented in 2000 the possibility of obtaining diffraction-limited flat lens from a negative index slab capable of perfect evanescent wave recovery at the image site[2].

Subsequently, through optical technology development, two types of man-made materials have been proposed by scientists. The first structure is a periodic arrangement of metallic split-ring resonators and thin wires for which concurrent negative permeability and permittivity can be demonstrated at the microwave frequency regime[3,4]. Despite the advantages of these metallic structures, metallic constituents suffer from serious losses at high frequencies[5]. The other structure is a periodic array of lossless dielectric materials called photonic crystals (PCs). Although the PC constituent elements are dielectrics with positive electric and magnetic responses to electromagnetic (EM) waves, PCs can behave as superlensing devices with an effective negative refractive index at infrared and visible frequency regimes[6], which are the important frequency regions in biomedical and nanoscale optical imaging, high-density optoelectronic devices, and optical communication technologies[7]. Negative refractions in PCs and LHMs are slightly different. In LHMs, when $n_{\text{eff}}=-1$, EM wave propagates through the background-LHM interface without any reflection[2]. By contrast, in dielectric PCs, depending on the incident mode of light and the main symmetries of the PC structure, light transmission through the PC can be prohibited.

In this letter, we investigate the possibility of obtaining negative refraction effect by a two-dimensional (2D) square lattice PC composed of germanium (Ge) cylinders with different radii in air background. Although imaging properties of several types of 2D-PCs have already been analyzed[8−11], optimization of the image resolution of the PC lenses by accurately and efficiently assessing newly designed structures[12−15] is still significant. The PC introduced in the current study benefits from a form factor and from suitably terminated surfaces. In calculating the band structure and simulating EM-wave propagation through PC, we employ the finite-difference time-domain (FDTD) method. The most remarkable feature of this structure is its compressed band diagram, which confirms all conditions required for effective negative refractive index (ENRI). Another important point is that the negative refraction effect is related to the frequency, which belongs to the second energy band around the Γ point with negative phase velocity. In our model system, this frequency is approximately $0.228(2\pi c/a)$, which is lower than the corresponding frequencies for the simple square and hexagonal PC lattices reported in previous studies[7,13,16−21]. In addition, spatial resolution of the PC lens and the influence of anti-reflective structure on image location and intensity of transmitted light are also studied in this letter.

The considered 2D-PC structure comprises a face-centered square lattice of infinitely long Ge cylinders, with different radii arranged in air background in the xy plane (Fig. 1). The permittivity of Ge is ε=18.0 at 1.55-μm wavelength, and the radii of the cylinders are R_1=0.3a and R_2=0.25a, where a is the lattice constant. These optimum values are found to reach the compressed band structure with complete band gap between the second and third energy bands upon examination of the different values for R_1 and R_2. We also set the lattice constant at 355 nm to examine the imaging properties of the 2D-PC structure at near-infrared frequency regime.

We have computed the PC structure band diagram using the FDTD method, which is based on the common Yee's algorithm for transverse magnetic (TM) polarization of EM wave along the most symmetrical lines (i.e., ΓX, XM, and $M\Gamma$) in the first Brillouin zone.

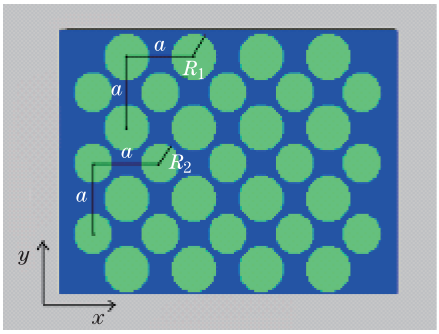

Fig. 1. (Color online) Schematic diagram of the 2D complex square lattice PC formed by Ge cylinders with radii R_1 and R_2 and lattice constant a.

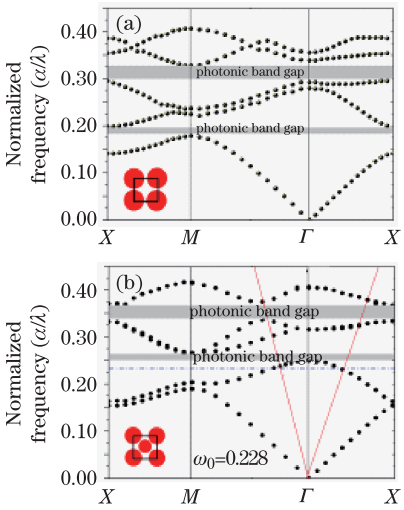

Fig. 2. (Color online) Photonic band diagram of (a) the conventional square lattice PC that consists of Ge cylinders with radius R=0.39a in air and (b) complex square lattice PC structure that is made from Ge cylinders with radius R_1 =0.3a and additional cylinders in the center of unit cell with R_2=0.25a. The solid lines depict the dispersion lines for air. Insets: unit cells of the PC structures.

Figure 2(a) shows the band structure of the simple square lattice PC, which is composed of Ge cylinders with radius R=0.39a. The band structure of the face-centered square lattice PC proposed in this letter is illustrated in Fig. 2(b). In this figure, the frequency is normalized by the factor $a/2\pi c$, where c is the speed of light in vacuum. The air-filling factors of both structures are both equal to 0.51. After evaluating the two band diagrams, we perceive that the face-centered square lattice compresses the PC band structure, removes the band gap between the first and second energy bands, and pushes the second band below $0.25(2\pi c/a)$ frequency. To avoid high-order Bragg diffractions inside the PC structure, the EM-wave frequency should be less than $0.5(2\pi c/a)$[22]. After appending the air-band diagram to the PC band structure, the intersection frequency is found at $0.228(2\pi c/a)$ around the Γ point in the second band. For frequencies that belong to the first energy band, production sign of the Poynting (S) and wave (k) vectors in the PC is positive; therefore, the PC behaves as a right-handed material. Additionally, the focusing effect occurs because of anisotropic dispersion in low frequencies, without any negative phase velocity[10]. According to Fig. 2(b), an inward gradient around the Γ point exists, and the group velocity of light is negative at $0.228(2\pi c/a)$ frequency. A key aspect of the face-centered square lattice is that the negative refraction frequency is much lower than the previously reported ones for the simple square and triangular lattices that are mostly around $0.3(2\pi c/a)$[7,13,16–21]. For a given light wavelength (λ) and a fixed PC structure with lattice constant a, higher resolution is obtained by decreasing a/λ[22]. Therefore, the lower the negative refraction frequency, the higher the image resolution of the PC lens[2,22].

To simulate image construction through this PC configuration, we select the $0.228(2\pi c/a)$ frequency, which corresponds to the intersection point of air and PC band structures. The TM-polarized EM-wave propagation through and beyond the structure has been simulated using the FDTD method, incorporating perfectly matched layer boundary condition. Figure 3 illustrates the electric field patterns of TM-polarized wave through the PC and the corresponding electric field intensity at its right side. The image construction by the PC lens is also observed in Fig. 3, but the intensity of light on the right side of the structure appears to be low. To overcome this problem, addition of anti-reflective structures to improve light transmission[23] and cutting PC slabs for surface mode excitation have been approved by scientists[24]. In the current study, we propose an anti-reflective structure on both sides of the PC, which is composed of an array of cylinders with radii R_3 and R_4 at a distance of d away from the PC. We also investigate their influence on the image position and the light intensity at the image site. Figure 4 shows the whole super-lens structure with proposed anti-reflective design. We examine the electric field distribution for different values of R_3, R_4, and separation distance d, we find that the optimum values of these parameters are R_3= 0.2a, R_4= 0.1a, and d= 0.5a, respectively. Figure 5 illustrates the electric field distribution of the point source operating at $0.228(2\pi c/a)$

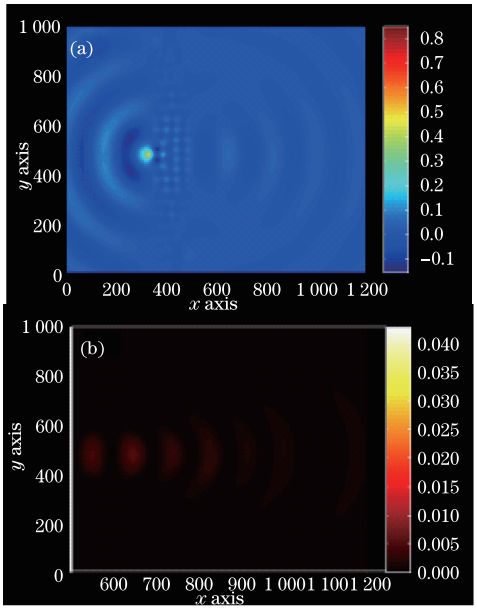

Fig. 3. (Color online) (a) Electric field distribution of a point source located at 0.75a from the left of the PC at normalized frequency of 0.228, and (b) the corresponding electric field intensity on the right side of the PC structure.

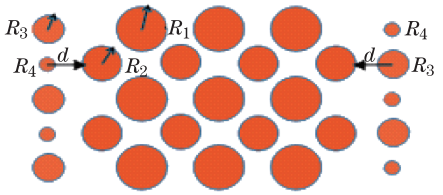

Fig. 4. (Color online) Complex 2D square lattice PC with asymmetric anti-reflector that consists of Ge cylinders with different radii R_3 and R_4 on both sides of the PC. Here, d represents the distance between the anti-reflector cylinders and the PC.

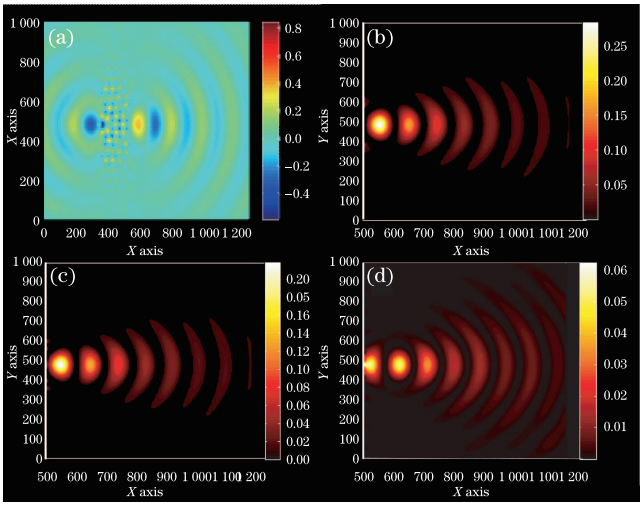

Fig. 5. (Color online) (a) Electric field distribution of a point source located at $0.75a$ from the PC with the asymmetric anti-reflector design composed of Ge cylinders with radii R_3=$0.2a$ and R_4=$0.1a$ on both sides of the PC structure; (b) corresponding electric field intensity on the right side of the PC; (c) electric field intensity for the PC with the symmetric anti-reflector design that is composed of Ge cylinders with optimum radii R_3=$0.2a$ and R_4=$0.1a$ on both sides of the PC structure; (d) simple anti-reflector made from cylindrical Ge rods with an optimum radius of $0.2a$ on both sides of the structure.

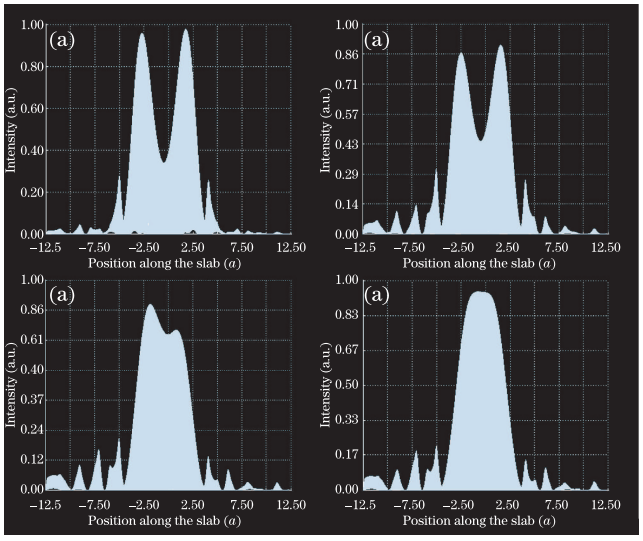

Fig. 6. (Color online) Electric field intensity related to the images of two point sources that are separated by a distance of (a) $4a$, (b) $3.5a$, (c) $3.2a$, and (d) $3.1a$.

frequency at a distance of $0.75a$ from the PC and the corresponding electric field intensity at the right side. Compared with Fig. 3, the composite anti-reflectors cause an obvious point image, and from Fig. 5(b), the light intensity at the image site is considerably increased. The anti-reflective structure increases the required interferences inside the PC, resulting in the apparent increase in light intensity at the image site.

The asymmetric design of the anti-reflective structure has a crucial function to obtain such focusing quality. The geometry and the selected radius of anti-reflector cylinders lead to more effective diffraction to enhance light intensity in the near-field zone. To verify this hypothesis, we have also considered two different conditions, i.e., a symmetric anti-reflector consisting of cylinders with radii R_3= $0.2a$ and R_4= $0.1a$, with separation distance d= $0.5a$, as well as a common configuration in which the optimum radii of cylinders at the surfaces are the same. Figure 5(c) shows the electric field intensity of the point source and its image for the case of the symmetric anti-reflector. Figure 5(d) depicts the electric field intensity distribution of the point source when radius R_4 is changed from $0.1a$ to $0.2a$, to create a simple anti-reflector. The point images constructed by these designs are evidently much clearer than that illustrated by Fig. 3. However, Figs. 5(c) and (d) clarify that the transmitted EM-field intensity at the focusing point is lower than that in Fig. 5(b). The light intensities at the image sites in Figs. 5(b), (c), and (d) are 0.28, 0.22, and 0.05 (in arbitrary unit), respectively. Another noticeable effect is that the asymmetric anti-reflective structure can also move the position of the image site by varying the radii of the cylinders, whereas the light intensity at the focus point still remains significant. These effects are ascribed to managing the EM-field interferences within the PC structure.

Spatial resolution in optical systems determines how closely lines can be resolved in an image, so a higher resolution means a more detailed image. To study the spatial resolution in the designed PC structure, we place two point sources $0.75a$ away from the PC with the asymmetric anti-reflector, such that they are vertically separated from each other by different distances. Considering that the point sources are assumed to be coherent with respect to each other, then the resolution can be improved because of the existence of the waves that add up in phase. To analyze the spatial resolution of the PC lens, we change the distance between the two point sources. Figure 6 depicts the light electric field intensity along the PC–air interface at the right side of the PC structure for different separations. When the distance between the two point sources is reduced to $3.1a$, one peak can be recognized. However, two peaks of images can be resolved at the separation distance of $3.2a$. In this case, in terms of the Rayleigh criterion, the resolution of the system is 0.7296λ, which is improved compared with the result that was recently achieved in annular PC flat lens[15].

In conclusion, based on the band structure analysis and the FDTD numerical modeling, we investigate super-lensing behavior in a complex 2D face-centered square lattice PC, comprising Ge cylinders arranged in air background. This complex structure creates a com-

pressed band structure, opens the first frequency gap between the second and third energy bands, and satisfies all conditions necessary to obtain a negative refraction effect. Compared with the previously studied PC lenses, the negative refraction frequency in the current study is considerably lower and belongs to the second energy band around the Γ point with negative phase velocity. With the introduction of novel anti-reflectors to both sides of the PC, we can improve the EM-wave transmission through the PC lens and make a high-quality point image. The image location can be moved away from the PC using different anti-reflective designs. In addition, we can reach a reduced spatial resolution using the present PC structure.

References

1. V. G. Veselago, Sov. Phys. Usp. **10,** 509 (1968).
2. J. B. Pendry, Phys. Rev. Lett. **85,** 3966 (2000).
3. A. K. Iyer and G. V. Eleftheriades, Appl. Phys. Lett. **92,** 131105 (2008).
4. J. M. Algarin, M. J. Freire, M. A. Lopez, M. Lapine, P. M. Jakob, V. C. Behr, and R. Marques, Appl. Phys. Lett. **98,** 014105 (2011).
5. M. Notomy, Phys. Rev. B **62,** 10696 (2000).
6. A. Sukhovich, B. Merheb, K. Muralidharan, J. O. Vasseur, Y. Pennec, P. A. Deymier, and J. H. Page, Phys. Rev. Lett. **102,** 154301 (2009).
7. J. Oden, M. Hofman, X. Melique, D. Lippens, and O.Vanbesien, Appl. Opt. **51,** 5601 (2012).
8. P. V. Parimi, W. T. Lu, P. Vodo, and S. Sridhar, Nature **426,** 404 (2003).
9. X. Wang, Z. F. Ren, and K. Kempa, Opt. Express **12,** 2919 (2004).
10. J. Li, M. H. Lu, T. Fan, X. K. Liu, L. Feng, Y. F. Tang, and Y. F. Chen, J. Appl. Phys. **102,** 073538 (2007).
11. T. Geng, T. Liu, and S. Zhuang, Chin. Opt. Lett. **5,** 361 (2007).
12. Y. Cui, V. A. Tamma, J. Lee, and W. Park, IEEE Photon. J. **2,** 1003 (2010).
13. H. Wu, L. Y. Jiang, W. Jia, and X. Y. Li, J. Opt. **13,** 095103 (2011).
14. S. Baek, A. V. Baryshev, and M. Inoue, J. Appl. Phys. **111,** 07E508 (2012).
15. F. Xia, M. Yun, M. Liu, J. Liang, W. Kong, H. Tan, and W. Lv, J. Appl. Phys. **113,** 013109 (2013).
16. Y. Fang and Z. Ouyang, Chin. Opt. Lett. **6,** 57 (2008).
17. J. L. Garcia-Pomar and M. Nieto-Vesperinas, Opt. Express **15,** 7786 (2007).
18. N. Fabre, S. Fasquel, C. Legrand, X. Melique, M. Muller, M. Francois, O. Vanbesien, and D. Lippens, Opto-Electron. Rev. **14,** 225 (2006).
19. W. Belhadj, D. Gamra, F. Abdelmalek, and H. Bouchriha, Opt. Quantum Electron. **37,** 575 (2005).
20. S. Feng, C. Ren, D. Xu, and Y. Wang, Chin. Opt. Lett. **7,** 849 (2009).
21. S. R. Dastjerdi, M. Ghanaatshoar, and T. Hattori, J. Opt. Soc. Korea **17,** 262 (2013).
22. C. Luo, S. G. Johnson, J. D. Joannopoulos, and J. B. Pendry, Phys. Rev. B **65,** 201104 (2002).
23. S. G. Lee, J. S. Choi, J. E. Kim, H. Y. Park, and C. S. Kee, Opt. Express **16,** 4270 (2008).
24. S. Xiao, M. Qiu, Z. Ruan, and S. He, Appl. Phys. Lett. **85,** 4269 (2004).